STRATEGIES AGAINST PARTICLE FOULING IN THE CHANNELS OF A MICRO HEAT EXCHANGER SUBJECT TO µPIV FLOW PATTERN MEASUREMENTS

V. Heinzel, A. Jianu and H. Sauter

Forschungszentrum Karlsruhe, Institut für Reaktorsicherheit, Postfach 3640, D-76021 Karlsruhe, Germany,
E-mail: sauter@irs.fzk.de

ABSTRACT

Our work in general aims at the measurement of flow patterns in the channels of micro devices like mixers and heat exchangers by **µPIV** (micro *Particle Imaging* Velocimetry). Therefore, the inherent present *particles* may cause *particle* fouling (**PF**), which is observed by the in turn inherent active *imaging* system. Simultaneously, it disturbs increasingly the measurement results, long before the flow will be blocked. Investigating the *roots of PF in micro* devices, and selecting appropriate *measures to mitigate* or delay it, was inevitable in order to achieve sufficient experiment run time. An exurb of that affords is presented in a mostly chronological order; a systematic fouling research concept is under preparation. Our findings involve the influence of *pumps, flow guidance, surface roughness* and *chemistry, fluid chemistry, supersonic disintegration* and particle aging by *agglomeration.* Cleaning procedures are a minor topic. The aptitude of µPIV in detecting early deposits and their impact on the flow is demonstrated.

INTRODUCTION

The task of this work is to visualize and measure flow patterns of liquids in and around the channels of miniature heat exchangers (Fig. 1), as they were developed in the Institute of Micro Processing (IMVT) of our Research Center (Schubert et al., 2001).

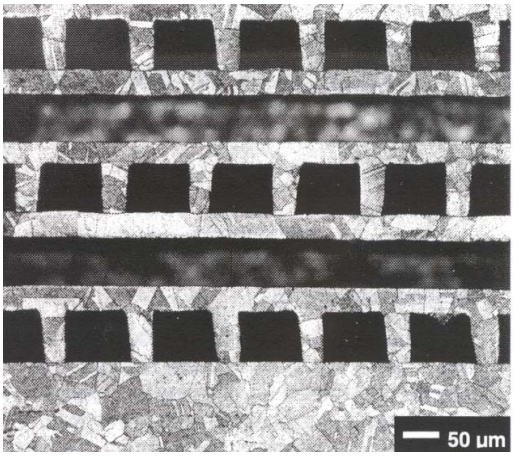

Fig. 1 Grinded cross section of an assembled and diffusion welded pile of cross flow heat exchanger slices

The investigation of the flow pattern aims, in a first step, at the laminar/turbulent transition; for microchannels, a wide range of Reynolds numbers is given. However, for predictions of pressure losses and heat transfer, the knowledge of the transition in dependence of the flow parameters is mandatory. Secondly, flow field data are needed for code validation.

The micro heat exchangers are composed of slices, into which the channels are engraved by grinding and cutting ribbons. The rectangular channels have typical widths of 100 to 200 µm and a height of about the same dimensions. Each slice has 34 parallel channels. Web walls about 100 µm broad separate the channels. The slice length in flow direction is about 14mm. The slices are piled up and diffusion-welded to a heat exchanger segment. Neighbouring slices have orthogonally directed channels, therewith, creating a cross-flow heat exchanger.

In our optical based experiments, single slices are used. As they are made out of metal, insight view into the channels is possible from top only, and care against reflections has to be taken, e.g. by use of fluorescent tracers. Traditional optical flow study methods like PIV and PT*(racking)*V are not directly applicable to such geometries, because they use orthogonal or through-light setups; volume illumination is a feasible approach. Previously implemented µPIV structures resemble that of an epifluorescent microscope (Santiago et al., 1998; Meinhart et al., 2000a-b; Kim et al., 2002; S. Devasenathipathy et al., 2003).

Compared to existing µPIV applications, our envisaged one aims at pressures up to 0.6 MPa, leading to flow velocities up to 15m/s and at temperatures up to 100°C. This entails higher time resolution, an objective with large working distance(*1) and certain precautions against leakages; some extra space for instrumentation has also to be foreseen (Heinzel et al., 2002).

EXPERIMENTAL TECHNIQUE

The Method: µPIV

Like in PIV, *particles* visualize as tracers, called seed, the flow of gases or liquids by light scatter, reflection or fluorescence. Two timely close up photos conserve the actual space distribution of the speed, with the component in depth to the image plane being given by scanning that

direction (unless stereoPIV is applied). In PIV, depth resolution is defined by the thickness of a light sheet; in μPIV this is replaced by the depth of focus, which should be small therefore. Otherwise, the speed of the objective should be high to allow for small particles and short illumination times. By the same token, the camera should not only be fast (*2), but also sensitive (Heinzel et al., 2003).

The pair of pictures may be pre-processed for suppressing underground, out of focus images or wall structure impacts. Then, (μ)PIV algorithms are applied; the most common ones divide the digitized pixel array into sub grids and perform a Fourier transform to each. By subsequently shifting pairs of sub grids relatively, the corresponding cross correlation value is generated; a value map yields, containing hopefully a clear maximum different from the always present zero shift peak. A reverse transform reveals amount and direction of the shift, which equals the average flow vector of the centre of the sub grid unless undue inhomogeneities there are present.

Microscope Set-up

The possibility to adjust the test object as well as the access to the measured samples stands in the foreground when deciding the μ-PIV geometry. Particle deposits should not be favored by the force of gravity.

Therefore, a lying optical-axis and a standing test object have been chosen. Additionally, this helps to avoid vibrations along the optical axis inasmuch the aspect ratio of the arrangement is kept as low as possible (Fig. 2).

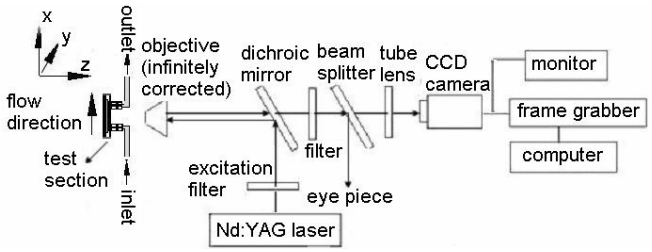

Fig. 2 Schema of our μPIV epifluorescent microscope

Test Loop Development

First approaches

A first setup consisted of an exclusively gravity driven water flow from an upper to a lower plenum through a horizontally mounted commercial test cell(*3). Both vessels had free surfaces with respect to the ambient. A *peristaltic* pump served for permanent reflow and constant fluid level in both vessels. The geodesic level difference of 1.40 m allowed for flow speeds of about 16 cm/s in a rectangular cell of 100 μm depth. This flow could be maintained without depositions for about 4 hours. Later on, more and more agglomerates passed through the cell and stuck to the walls, mainly to the ceiling. As the cell inlet was at its bottom, perpendicularly directed to the ceiling, a ring of deposits built up *opposite to the inlet,* influencing the flow pattern up to throttling the flow. This could largely be avoided by manufacturing a bottom plate of 6 mm thick carbon-enhanced Teflon with inlet- and outlet channels placed slightly *inclined* to the ceiling (Fig.3).

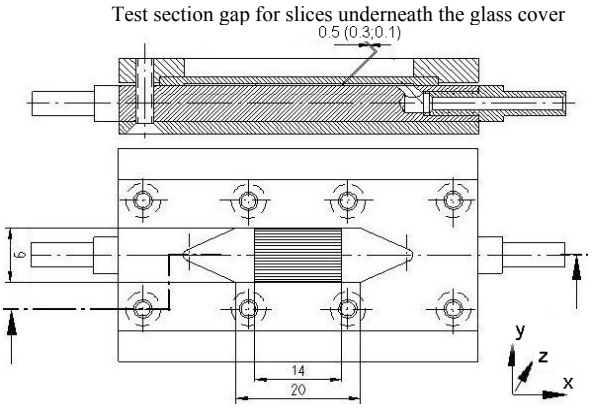

Fig. 3 Slice holder with *inclined flow guidance* at inlets

Next, agglomerates were formed at the *silicon* walls of the hoses in the *squeezing* zone of the peristaltic *pump*, some of them remaining and others becoming volatile and causing error signals which increased with time in intensity and frequency.

Advanced drive

With respect to PF, the flow driving element of the test loop was replaced. The circulation became induced by a section with mixed rising bubbles. A stable sequence of rising bubbles (plug flow) in an upward hose could be reached by a sufficient high bubble frequency together with a mixing ratio of air to fluid of about 3 or 4 to one, thereby creating a circulating feed flow to the top collecting vessel. The resulting "bubble *pump*" could be operated unattended for days. The main advantage of this kind of pump is the absence of moving parts producing *shear stress* causing PF (apart from the phase interfaces) (Fig.4).

Applying particles or chemicals as well as taking probes could be comfortably done via the open surface underneath the lab ceiling; excessive foaming had to be prohibited. In the long run, a minor deposition of agglomerates in the funnel cone could be observed, suggesting that here the *bubble-fluid surface escape* process was the main PF inducing cause.

Advanced slice holder and slices

The test structure used in the next measurements consisted of a flat cell milled into a carbon enhanced Teflon bottom, into which the micro heat exchanger slice was

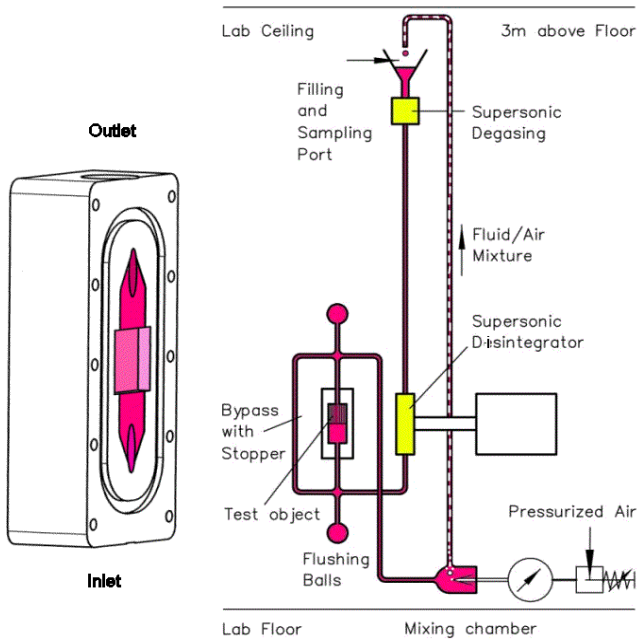

Fig. 4 Test loop with bubble pump and new slice holder, magnified on the left side
(red: fluid; yellow: supersonic devices)

embedded in a separate milled deepening (Fig. 5). The flat cell had an inlet channel of 25 mm length, and a smooth top covered with a glass plate. In this way, a nearly straight flow transition from the inlet flat channel into the channels of the slice could be maintained, with a certain unavoidable transition dip stemming both from the uptake manufacture tolerance and the slice *end cutting deformation* (Fig. 7).

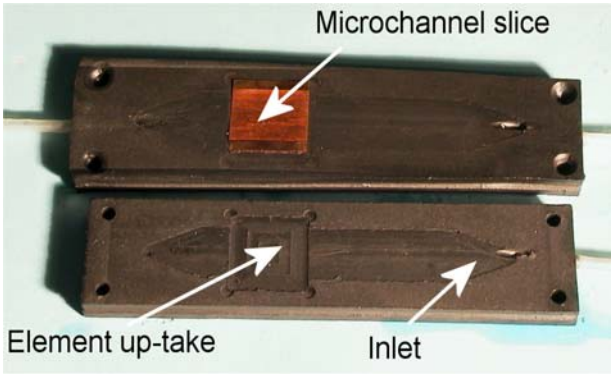

Fig. 5 Test structure with and without microchannel slice

Different models of heat exchanger slices became in use, with channel profiles varying from 100 to 200 µm depth and 100 to 500 µm width, out of different materials and with different *surface roughness*. Meanwhile, special care has been taken to the last parameter due to PF.

Details can be seen in Fig.6, showing a front view on the inlet/exit zones of different generations and types of slices. The lowest one is a stainless steel made, 200 x 200 µm type of the first generation, resulting in poor suitability for µPIV measurements. The upper one is also made of stainless steel, 100 x 100 µm, but with *much smoother* wall and bottom structure.

First useful µPIV results could be obtained using this specimen. The results reported here stem from the third generation of heat exchanger elements (copper made, 100 x 200 µm), shown in the middle of Fig. 6. Due to a different, for µPIV measurement specially designed milling procedure, the web wall, top and bottom surfaces appeared nearly *mirror-like smooth*. The ends only showed some *cutting marks* and a slight *deformation*.

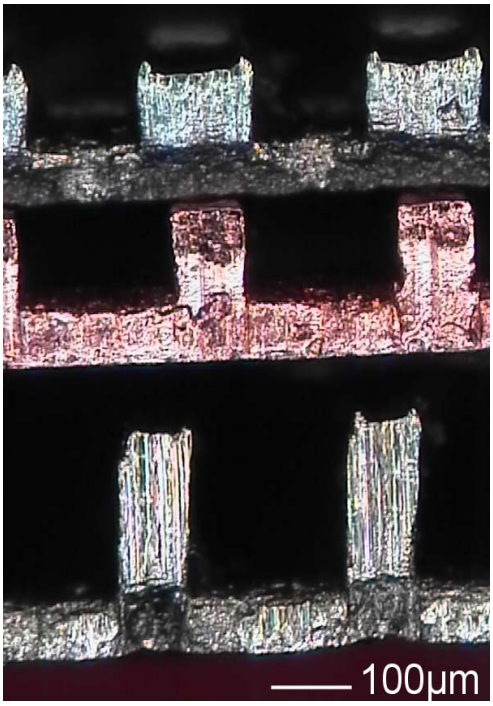

Fig. 6 Three generations of heat exchanger slices,
- front view of the inlet-outlet ends
(channels inside, web walls, bottom plate)

Particles

Preliminary tests showed that particle size and density should be adapted to the foreseen velocity range. Small particles are able to follow the flow in the microchannels, not only in the laminar but also in the laminar-to-turbulent transient phase. Larger ones yield more brightness. For seeding, 0.7 µm diameter fluorescent polystyrene spheres and a seed density of 2.2 x 10^6 particles/mm^3 were chosen.

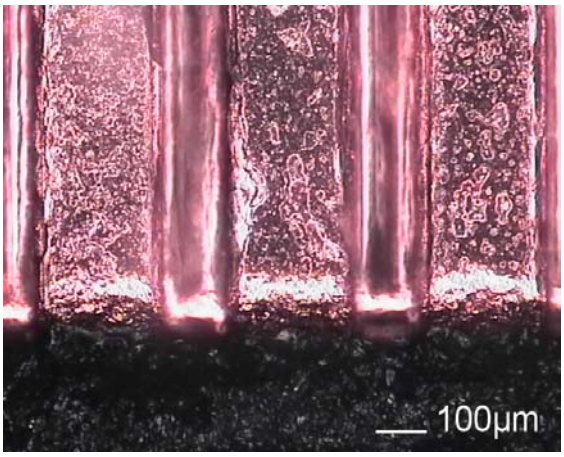

Fig. 7 Top view of the actual element embedded into the Teflon basement. The transition dip both in uptake and element end can be seen as deeper layers that are slightly out of focus.

Fluid Treatment

Basic

The volume of the loop was ~50ml and we began with deionized water with added particle suspension (typically 2 ml), relying completely on the anti-coagulation chemical mixture of the manufacturer(*4); later on we added various *alcohol compounds* for delaying agglomeration.

A home-made miniature *supersonic disintegrator* placed immediately at the funnel outlet (assuming that the major fraction of new aggregates came into existence here) caused a considerable delay in the built-up of large agglomerates and of early depositions. A novel type of powerful supersonic disintegrator(*5) operating a 4mm diameter times 20 cm length flow through type glass tube in the cavitations regime (originally developed for a totally different application) turned out to efficiently disintegrate all agglomerates and was therefore placed immediately in front of the test cell inlet. The first home-made disintegrator remained in action in order to degas the fluid, allowing bubbles to escape via the funnel.

Advanced fluid treatment

Better avoidance of deposition and possibly removal of weakly fixed deposits could be produced by compressing the surface attraction potential curve using e.g. triphospates. The most effective and still low concentrated *recipe* consisted in 2% isopropanol, about 2 weight% penta-sodium triphosphate (corresponding to a resulting pH of 7.5), traces of Triton X-100 (*6) and even tinier ones of silicone antifoaming emulsion. Most likely, the amount of *additives* can further be considerably reduced due to the effectiveness of the disintegrator now in use. This recipe, however, seemed to be in some transient *incompatibility* to the seed particle manufacturer's own anticoagulation recipe used in the carrier fluid for shipment endurance, which is unknown to the customer. When adding thoroughly homogenized particle suspension to the prepared clean loop, a sudden enhanced coagulation starts up, disappearing soon later. In this early phase, the channels of the test elements may be contaminated durable unless bypassed.

With that *management*, the loop could be operated for more than 6 hours without any deposits in the channels and only minor ones in the channel inlet regions. Clogging did not occur even within 48 hours, but losses in signal strength were observed. This might be due partly to particles lost by sticking to the walls anywhere in the loop as well as to photo bleaching of the fluorescent dye of the seed.

PROGRESS IN PF AFFECTED µPIV MEASUREMENTS

First µPIV results were obtained in a empty (*no slice* inserted) flat cell according to fig. 8 (cell depth 500 µm). The shown measurements were performed in the neighborhood of the cell inlet, which explains the fact that the flow direction differs from *x* direction. The measurement plane was placed close to the cell surface. The decline is due to the intended slight tilt of the camera chip ground line to detect artifacts such as vibrations, etc.

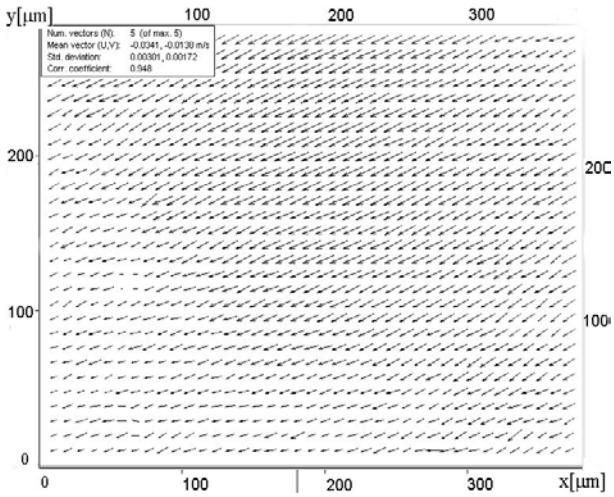

Fig. 8a Vector map showing direction and magnitude of the flow velocity in the empty flat cell

The situation changed remarkably when a slice of stainless steel, first generation, was inserted into the test cell, forcing the flow through 34 parallel channels of 200 x 200 µm of 14 mm length. The *scratches* in the microchannel walls and bottom, stemming from the manufacturing process, were soon tinted with fluorescent particles - not necessary agglomerates - (see Fig. 9a), which produced

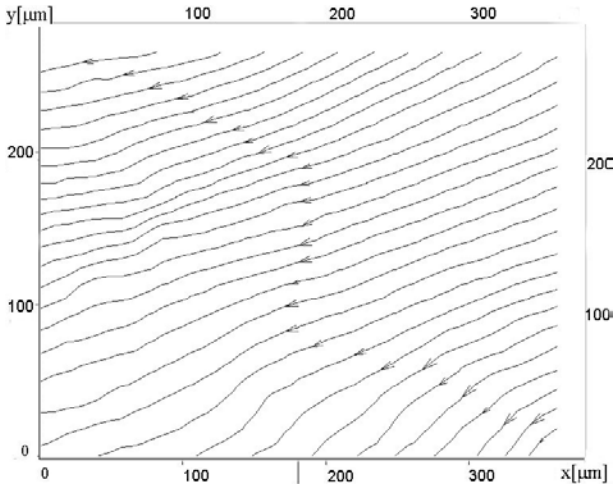

Fig. 8b Streamlines in the empty flat cell

a *slowly changing background* pattern (constant, in terms of µPIV *exposure* times) representing a zero flow velocity. When applying µPIV algorithms to pairs of particle images of this type, the resulting "vectors" would represent the structure of the channel rather than the pattern of the flow.

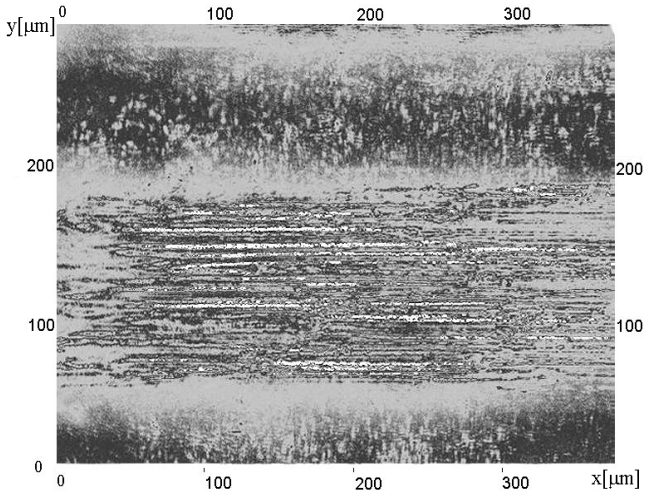

Fig. 9a Particle rough image in the microchannel (strong background and noise due to particle accumulation in the wall scratches)

In the vector map, the inlet rim of the channel plate at about 150 µm from the left border, as well as the channel side walls can be guessed (Fig. 9b. Arrows help the unfamiliar viewer to detect a remainder of order hidden in the chaos.)

In spite of PF limited run time, with the knowledge of appropriate µPIV experimental parameter settings, together with an improved slice, it was possible to have sense making

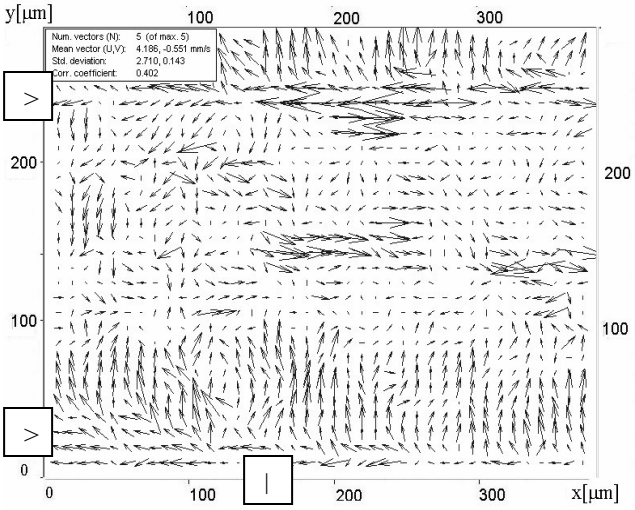

Fig. 9b "Vector" map obtained by applying the (µ)PIV algorithm to images as shown in Fig. 9a

recordings of the *onset of inlet plugging* shown in Fig10 a,b. The software calculated "streamlines" are rough estimates only, rather than scientific consistent elaborates.

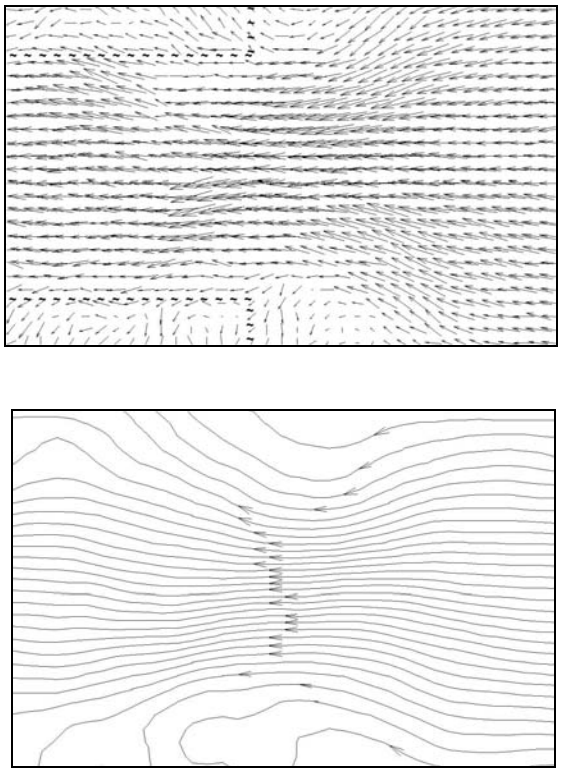

Fig. 10a,b: Onset of inlet plugging by PF, dashed lines denote channel inlet and side walls. Scales as above.

Altogether, the preliminary runs show the aptitude of the setup to produce sensible results as long as PF remains insignificant to the optical appearance of the test section. Therefore, avoiding or remedying the impacts of PF is the major key to µPIV application in closed circuits.

µPIV RESULTS OF ADVANCED VERSIONS

Procedure and Scales

The image fields were analyzed using the DANTEC FlowManager software by ensemble averaging the velocity vectors after correlation peak detection. Domains in the instantaneous fields, where valid vectors could not be obtained, were excluded from the averaging. The ensemble-averaging technique could be applied due to the fact that the flow to be measured was a steady one (and not affected by PF). For the current experiment, 20 realizations were sufficient to give a good signal, and, as can be seen in the presented results, the number of erroneous velocity measurements (i.e. missing or false vectors) is tolerable (no additional vector validation or velocity field smoothening tools were applied in this presentation).

µPIV measurements of the flow within one channel (Fig. 11a) were evaluated at the channel entrance (b) and downstream (c) where the flow is fully developed. The centreline of the channel, respectively of the web wall, gives the origin of the x-axis. The origin of the y-axis is given by the element inlet borderline (cf. dashed lines). The measure-ment series shown in Fig. 11 aimed at the visualization of the transition from the uniform flow in the flat cell into a channel and the flow development along the axis.

The measurement volume presented here is located 42µm below the top glass cover. The data in these plots were obtained with a time delay of 50 µs between image pairs. On average, the µPIV interrogation volumes used here each contained about 50 particles. The Reynolds number of based on hydraulic diameter and volume-averaged velocity is approximately 5, which roughly applies also to the above published flow maps.

Outcome

In Fig. 11c, the uniformity of the velocity profiles along the axial direction shows the fully developed flow existing already at a stream wise distance of approximately 0.75 hydraulic diameters from the channel entrance. Sensible measurements were obtained to within 7.5 µm distance to the wall.

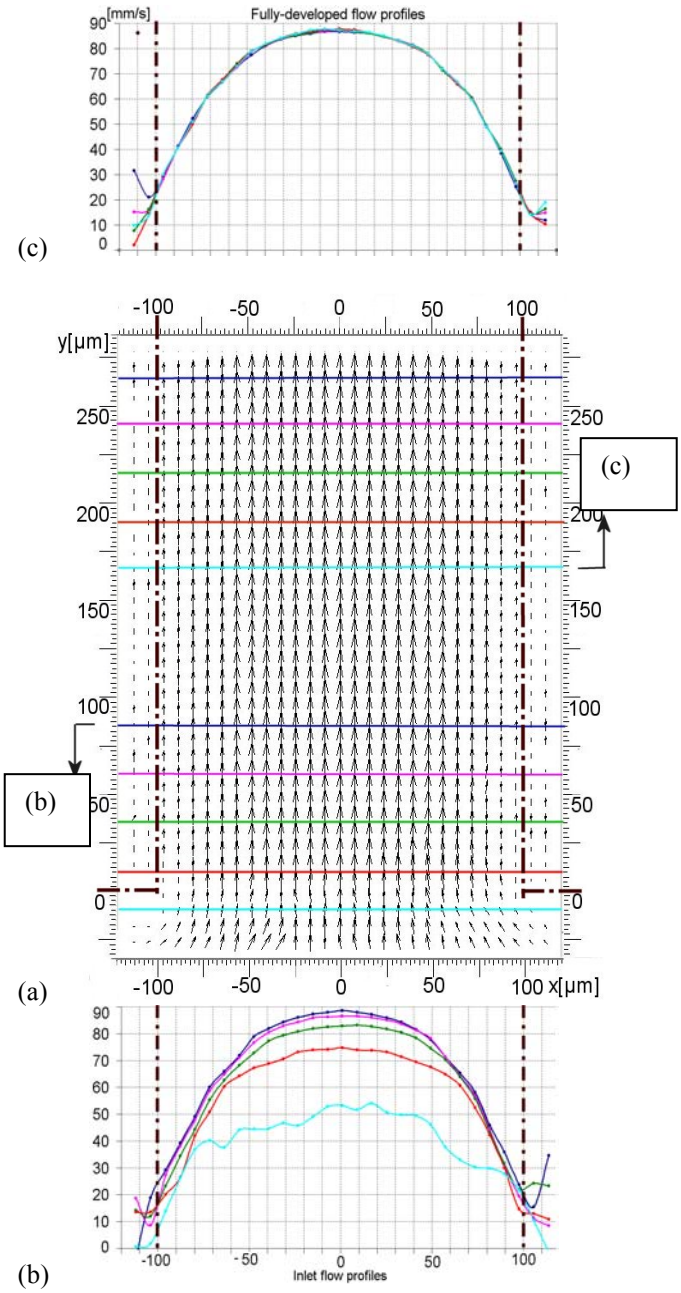

Fig. 11 µPIV measurements of the flow within one channel at a depth of 42 µm (channel inlet and downstream): (a) flow map; colour bars indicate corresponding profile position;--profiles near inlet, strong changing (b) below, and fully developed downstream (c), top. (see arrows in a)

This time switched as a *two-stage*, three parallel channel pump with a pressurized *air buffered damping* volume. At pressures of 0.11MPa, maximum channel centre flow *speeds of 1m/s* could be reached (Fig. 12c). However, the chemical cocktail must be very carefully mixed and the supersonic disintegrator must be operated at 50% power (vs.

Third (Intermediate) Setup and Results

In a ***most recent technical*** experiment, the aptitude of the test object holder to withstand *higher pressures* was the aim of the investigation. For that purpose, regardless of bad PF influence, the *peristaltic* pump was used again.

20% in the previous experiments). Both were *not* done at optimum. Therefore, due to the repeated use of the *peristaltic* pump, deposits occurred by 2h.

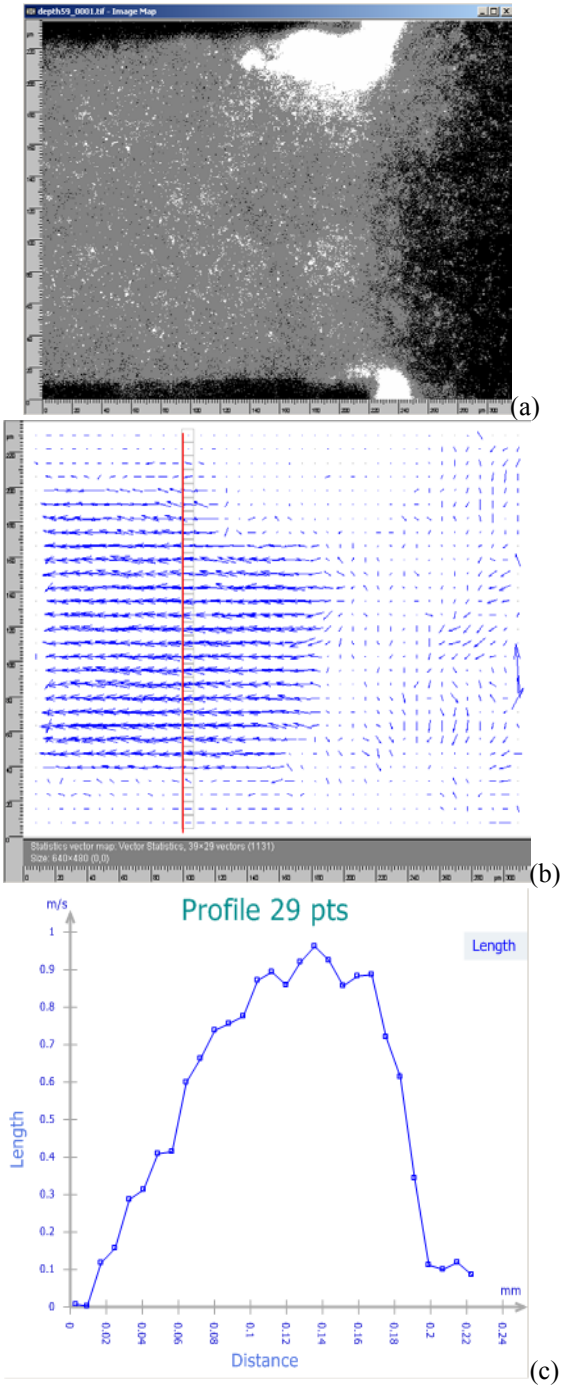

Fig. 12: Progressed channel inlet plugging at *higher* speeds; (channel inlet on the right, channel mid-depth): (a) rough picture, (b) vector map, (c) velocity profile along the red line in (b).

It can be seen from the vector map (Fig. 12b) that vectors are missing because the flow in the inlet region is not steady enough to deliver good results when *averaging* by ensemble correlation technique. The vector map recovers as well, that the progressed deposits, as depicted in Fig. 12a, concentrated at *higher speeds* at the very *inlet*, influence remarkably the flow pattern also down streams.

STRATEGIES LEARNED AGAINST PF IN µSYSTEMS

It is important that as few particles as possible coalesce in order that very few *agglomerates* form in the closed circuit. As already mentioned, there are several reasons which make this behavior important:

- *agglomerates* may much easier stick to the walls of the microchannels and remain there than the primary particles, spheres of 0.7 µm in diameter;
- when present in the test cell, they may change *stochastically* the characteristics of the flow, rendering averaging obsolete;
- their presence contributes in the recorded images to *timely irregularities* of the undesired *background* that thus cannot be compensated for;
- they will influence the flow *distribution* between the individual channels and finally *block* one by one.

When *starting* an experiment with a *clean* test circuit, the following actions are suggested to be undertaken in order to expand the available measurement time:

- suitable fluid *chemistry* selection with respect to the particle-surface nanostructures (and near forces);
- chemical *surface* functionalizing both for the particles and for the cell walls (glass cover);
- choice of suitable *materials* in the loop (silicon avoided and Teflon most preferred) ***and !***
- *reducing* the number of *different* materials in the loop;
- avoidance of *geometrical* structures giving rise to *shear* stress in the flow (e.g. *sharp rectangular* bents);
- avoidance of certain regular *roughness* structures;
- applying of *supersonic* fields of local well distributed and suited energy density (cavitation);
- filtering techniques with the appropriate cutoff characteristics (preparation/standby);
- *time management* with respect to setup, adjustment and *active measurement* as well as *guarded* standby phases.

Much work has been done in order to find out the best possible *cleaning* methods for degraded test cells. To reactivate a loop/test section without *dismantling* it, the following actions were undertaken:

- *rinsing* using a lot of combinations of additives; the best of them removed no more than ~90% of the

depositions (a lengthy rinsing using distilled water must follow to remove the additives themselves which, if present, influence the fluid characteristics);
- *pressure* flushing, *pulsed* flushing, *reverse* flushing (hardly removes the depositions left after rinsing);
- mechanical cleaning by flushing with particles mixed with (fibers, sand, large latex spheres) – still under investigation; it proved partly to be successful but it implies risks and drawbacks like scratching, plugging, changing flow conditions; *gas bubbles* seem to be an alternative;
- applying supersonic field – is widely dependent on the source-loop coupling and presents the drawback that the sealing might be destroyed.

All methods which were applied until now could improve the quality of the optical output for a *limited* time. They were not able to reestablish the *initial performance* the loop showed when freshly reassembled with separately cleaned and/or renewed components. µPIV shows to be much more sensitive even to a slight onset of fouling and to remainders from cleaning processes in comparison with the extensively investigated particle fouling impact on heat exchange.

CONCLUSIONS

As far as PF is concerned, our findings are:
- The 0.7µm tracer spheres *themselves* do not contribute to fouling. Instead, they *form aggregates* which do.
- Most fouling occurs at the *channel edges*, at the *inlet* web wall and at *roughness*, as well as at each *sharp* bent.
- A considerable contribution stems from tiny *fibres*, partly of sub microscopic diameter, which act as agglomerate *catchers*. They come into existence even in pure deionate if *stored* for a while and is used unfiltered.
- The *chemical cocktail* turned out to be effective as well as the *supersonic disintegrator*. Both measures work synergetic.
- A special effect is the short term and *transient incompatibility* of our own chemical recipe with the unknown manufacturer's cocktail used for shipment of the particle concentrate. By *mixing*, the phase of enhanced agglomeration expires.
- A really satisfactorily working *cleaning* process of the undismantled test section could *not* be found. Small onsets of deposits could be removed, but the reached lifetime was *shorter* than that of a new test cell or one that was cleaned after dismantling.

REFERENCES

K. Schubert, L. Brandner, M. Fichter, G. Linder, U. Schygulla and A. Wenka, 2001, Microstructure devices for applications in thermal and chemical process engineering, *Microscale Thermophysical Engineering*, Vol. 5, pp. 17-39.

J. G. Santiago, S. T. Wereley, C. D. Meinhart, D. J. Beebe, R. J. Adrian, 1998, Particle Image Velocimetry System for Microfluidics, *Experiments in Fluids*, Vol. 25, pp. 316–319.

C. D. Meinhart, S. T. Wereley, M. H. B. Gray, 2000a, Volume Illumination for Two-dimensional Particle Image Velocimetry, *Meas Sci Technol*, Vol. 11, pp. 809–814.

C. D. Meinhart and H. Zhang, 2000b, The flow structure inside a micro fabricated inkjet print head, *J. of Microelectromechanical Systems*, Vol. 9, No.1, pp. 67-75.

M. J. Kim, A. Beskok and K. D. Kihm, 2002, Electro-osmosis-driven micro-channel flows: A Comparative Study of Microscopic Particle Image Velocimetry Measurements and Numerical Simulations, *Experiments in Fluids*, Vol. 33, pp. 170-180.

S. Devasenathipathy, J.G. Santiago, S.T. Wereley, C.D. Meinhart, K. Takehara, 2003, Particle Imaging Techniques for Microfabricated fluidic systems, *Experiments in Fluids*, Vol. 34, pp. 504-514.

V. Heinzel, U. Imke and H. Sauter, 2002, experimental and numeric Investigations on Flow Regimes and Heat Transfer in Micro Heat Exchangers, *Nachrichten-Forschungszentrum Karlsruhe*, Jahrg. 34, 2-3/2002, pp. 129-136.

V. Heinzel, A. Jianu, H. Sauter, *1st Int. Conf. on Microchannels and Minichannels,* April 24-26 (2003), Rochester, NY, USA, ICMM2003-1121

List of Manufacturers

*1:Microscope Objectives, large working distance:
Mitutoyo M PLAN APO by Edmund Optics,Inc;
OPTEM Super 10X , Avimo Precision Instruments
*2:PIV-CCD Camera:
Sensicam Double Shutter by PCO Computer Optics GmbH, D-93309 Kelkheim
*3:Test Cell:
Demontierbare Küvetten by Hellma GmbH & Co. KG D-79371 Müllheim (Hellma Worldwide)
*4:Seed, Particles, Fluorescent Microspheres, Beads:
Duke Scientific Corp. by Distrilab B.V. The Netherl.
*5:Supersonic Flow Through Disintegrator:
dr. hielscher GmbH, D-14513 Teltow
*6:Chemicals, esp. Triton X 100:
Merck KGaA, D-64293 Darmstadt